JMS

SPECIAL FEATURE:
PERSPECTIVE

The Orbitrap: a new mass spectrometer

Qizhi Hu,[a] Robert J. Noll,[a] Hongyan Li,[a] Alexander Makarov,[b] Mark Hardman[c] and R. Graham Cooks[a]*

[a] Purdue University, Chemistry Department, West Lafayette, IN 47907, USA
[b] Thermo Electron (Bremen), Hanna-Kunath-Str. 11, Bremen 28199, Germany
[c] Thermo Electron (San Jose) 355 River Oaks Parkway, San Jose, CA 95134 USA

Research areas such as proteomics and metabolomics are driving the demand for mass spectrometers that have high performance but modest power requirements, size, and cost. This paper describes such an instrument, the Orbitrap, based on a new type of mass analyzer invented by Makarov. The Orbitrap operates by radially trapping ions about a central spindle electrode. An outer barrel-like electrode is coaxial with the inner spindlelike electrode and mass/charge values are measured from the frequency of harmonic ion oscillations, along the axis of the electric field, undergone by the orbitally trapped ions. This axial frequency is independent of the energy and spatial spread of the ions. Ion frequencies are measured non-destructively by acquisition of time-domain image current transients, with subsequent fast Fourier transforms (FFTs) being used to obtain the mass spectra.

In addition to describing the Orbitrap mass analyzer, this paper also describes a complete Orbitrap-based mass spectrometer, equipped with an electrospray ionization source (ESI). Ions are transferred from the ESI source through three stages of differential pumping using RF guide quadrupoles. The third quadrupole, pressurized to less than 10^{-3} Torr with collision gas, acts as an ion accumulator; ion/neutral collisions slow the ions and cause them to pool in an axial potential well at the end of the quadrupole. Ion bunches are injected from this pool into the Orbitrap analyzer for mass analysis. The ion injection process is described in a simplified way, including a description of electrodynamic squeezing, field compensation for the effects of the ion injection slit, and criteria for orbital stability. Features of the Orbitrap at its present stage of development include high mass resolution (up to 150 000), large space charge capacity, high mass accuracy (2–5 ppm), a mass/charge range of at least 6000, and dynamic range greater than 10.[3]

Applications based on electrospray ionization are described, including characterization of transition-metal complexes, oligosaccharides, peptides, and proteins. Use is also made of the high-resolution capabilities of the Orbitrap to confirm the presence of metaclusters of serine octamers in ESI mass spectra and to perform H/D exchange experiments on these ions in the storage quadrupole. Copyright © 2005 John Wiley & Sons, Ltd.

INTRODUCTION

Need for high performance instrumentation

A major driving force for innovation in mass spectrometry in the past few decades has been the needs of bioanalytical chemistry. Genomics, proteomics, and metabolomics increasingly require the analysis of extremely complex mixtures, such as whole-cell lysates, and detection of analytes of a wide variety of types over a wide range of concentrations—from hormones and growth regulators present at pmole/L levels to ubiquitous as well as rare low copy number proteins. These challenges increasingly demand instruments with better performance characteristics including resolution, mass accuracy, dynamic range, and tandem mass spectrometry capabilities. They are also forcing the introduction of new analytical criteria involving multiplexing, differential measurements, data-dependent data acquisition, and automation.

Mass spectrometric analysis of complex mixtures for particular analytes is often facilitated by tandem or multiple-stage mass spectrometry (MS^n) as well as by high-resolution/high-mass accuracy measurements. The value of multiple-stage mass spectrometry is well established, both for characterization of particular compounds using product ion scans and for recognizing members of classes of compounds using neutral loss[1] or gain scans,[2] and precursor ion scans.[3] Methods like collision-induced dissociation (CID) and surface-induced dissociation (SID) are needed to activate molecular ions to generate characteristic fragments in these MS/MS experiments. Characteristic fragments are essential for establishing amino acid or sugar sequences and thereby allowing the inference of peptide, protein, or glycoprotein structures.[4,5]

Accurate mass measurement, coupled with sufficient resolution, makes it possible to greatly restrict the enormous number of possible molecular formulas that might be represented by a particular molecular mass. Mass measurement accuracy of 10 ppm allows useful measurements of molecular formulas, although 1 to 2 ppm is preferable. Sub-ppm values are now provided by traditional double-focusing sector instruments in the peak matching experiment[6] and by Fourier Transform-Ion Cyclotron Resonance (FT-ICR) instruments.[7] Time-of-flight (TOF) mass spectrometers have begun to provide 2 to 5 ppm accuracy.[8,9] Quadrupole ion trap mass measurement accuracies are at best 20 ppm,[10] a singular limitation on the value of these otherwise very versatile devices.

Orbital trapping and Kingdon traps

Mass spectrometry is unique among instrumental methods of analysis in that several different physical principles form the basis for its successful implementation.[11,12] Mass/charge analysis can be based on the measurements of momentum in magnetic sector[13] and kinetic energy in electrostatic sector instruments,[14] path stability in linear quadrupoles,[15] orbital frequency in both ion cyclotron resonance mass spectrometers[7,16,17] and quadrupole ion traps,[18] and velocity in time-of-flight instruments.[19,20] Each method has its own strengths and weaknesses. Analyzers can be grouped into classes on the basis of many properties, including ion beam versus ion-trapping types, continuous versus pulsed analysis, operation using low versus high translational energy ions, and on the basis of the time scale of the analysis and the pressure required for optimum performance.

The Orbitrap mass analyzer, the subject of this paper, bears a similarity to an earlier ion storage device, the Kingdon trap, as well as to two types of ion-trapping mass analyzers, the Paul trap (quadrupole ion trap), and the Fourier transform ion cyclotron resonance instrument. The first step in the set of inventions that led to the Orbitrap was the implementation of orbital trapping, a method of ion trapping, which can itself be used for mass analysis. The Kingdon trap, named after its inventor,[21] utilizes a purely electrostatic field for ion trapping, using neither magnetic nor dynamic (RF) electric fields. It consists of a thin-wire central electrode, an electrically isolated coaxial outer cylindrical electrode, and two endcap electrodes. A DC voltage is applied between the outer and inner electrodes, producing a radial logarithmic potential between the two electrodes.

$$\Phi = A \, lnr + B \qquad (1)$$

Here r is the radial coordinate, and A and B are constants. The axial field component due to the endcap electrodes and cross-terms between r and z are neglected in Eqn 1. If ions are created inside the trap, or introduced into it with a velocity perpendicular to the wire electrode, those with appropriate perpendicular velocities will move in stable orbits around the central electrode. Application of a potential to the endcap electrodes can be used to achieve simultaneous ion trapping in the axial direction. The Kingdon trap has been used to study molecular beams[22] and to develop the orbitron ion pump.[23] It has been used widely for trapping ions in studies of ion optical spectroscopy.[24,25] Trapping times of a few seconds for singly charged molecular ions can be achieved in the Kingdon trap.

In 1981, Knight modified the shape of the outer electrode of a Kingdon trap to produce an axial quadrupole term, in addition to the radial logarithmic term, in the electric potential.[26] The pure quadrupole potential, for example, in a quadrupole ion trap (QIT), is[18]

$$\Phi = A(z^2 - r^2/2) \qquad (2)$$

The modified potential for Knight's quadrupole/Kingdon trap is approximately represented by Eqn 3.

$$\Phi = A(z^2 - r^2/2 + B \, lnr) \qquad (3)$$

Here, r and z represent the cylindrical coordinates (the plane of symmetry of the potential is $z = 0$), while A and B are constants associated with the particular Kingdon trap geometry and the applied voltages. The logarithmic potential between the outer and central electrodes provides orbital ion trapping in the radial direction, as in the traditional Kingdon trap, while the quadrupolar potential confines ions axially, allowing them to undergo harmonic oscillation in the z-direction. Quadro-logarithmic fields have been used prior to this by others in energy analyzers[27] and proposed for use in time-of-flight mass analyzers.[28]

Knight used the trap to monitor ions produced by pulsed laser ablation of solid targets. The outer electrode was split at the middle ($z = 0$), allowing ions to be injected into the trap. The device could be used to monitor trapped ions by (i) measuring the time-dependent ion current due to continuous axial loss, or (ii) pulsing the central wire electrode positive and collecting the radially ejected ions. The axial potential is harmonic; so applying an AC frequency between the split outer electrodes allowed the observation of resonances in both the axial and radial ion signals. However, in both cases, observed resonances were considerably weaker, broadened, and shifted in frequency compared to those observed in a pure quadrupole ion trap. No mass spectra were reported for the device. Knight proposed that the central wire might distort the quadrupolar nature of the axial potential, which suggests that additional

cross-terms in r and z may be needed in Eqn. 1 to fully describe the potential. Other modified Kingdon traps have also been reported, including a version with two parallel wires[29] and another modification known as the 'dynamic Kingdon trap',[30] involving superimposing an AC voltage onto the DC potential to improve trapping efficiency.

Orbitrap mass analyzer

Makarov invented a new type of mass spectrometer, the Orbitrap,[31–33] illustrated in Fig. 1. Although a wholly new mass analyzer, for didactic purposes it is useful to consider the Orbitrap as a modified 'Knight-style' Kingdon trap with specially shaped inner and outer electrodes. Similarly, it can also be considered as a modified form of quadrupole ion trap, although the Orbitrap uses static electrostatic fields while the quadrupole ion trap uses a dynamic electric field typically oscillating at ~1 MHz.[1] The Orbitrap's axially symmetric electrodes create a combined 'quadro-logarithmic' electrostatic potential:

$$U(r, z) = \frac{k}{2}\left(z^2 - \frac{r^2}{2}\right) + \frac{k}{2}\cdot(R_m)^2\cdot \ln\left[\frac{r}{R_m}\right] + C \quad (4)$$

Here, r and z are cylindrical coordinates, k is a constant, k is field curvature, and R_m is the characteristic radius. Stable ion trajectories involve both orbiting motion *around* the central electrode (r, φ-motion, where φ is the angular co ordinate) and *simultaneous* oscillations in the z-direction. As is evident from Eqn. 4, the specially shaped electrodes
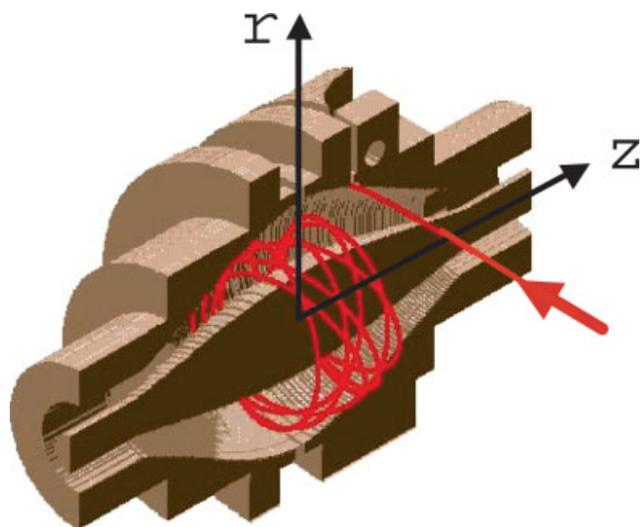

Figure 1. Cutaway view of the Orbitrap mass analyzer. Ions are injected into the Orbitrap at the point indicated by the red arrow. The ions are injected with a velocity perpendicular to the long axis of the Orbitrap (the *z*-axis). Injection at a point displaced from *z* = 0 gives the ions potential energy in the *z*-direction. Ion injection at this point on the *z*-potential is analogous to pulling back a pendulum bob and then releasing it to oscillate.

[1] Details in ion injection, including excitation by injection away from the equator, *z* = 0, and centrifugal squeezing, further distinguish the Orbitrap from these other devices. See References 31 and 33 for more detailed discussion of these subjects.

produce an electrostatic potential containing no cross-terms in r and z. Thus, the potential in the z-direction is exclusively quadratic. Ion motion along the z-axis may be described as an harmonic oscillator and is completely independent of r, φ motion. Ion mass/charge ratio m/z is simply related to the frequency of ion oscillation along the z-axis.

$$\omega = \sqrt{(z/m)\cdot k} \quad (5)$$

Makarov has previously described the equations of motion in considerable detail.[32]

In an analogy with what is done in yet another type of mass spectrometer, the FT-ICR, ion detection is performed by broadband image current detection, followed by a fast Fourier transform (FFT) algorithm[34] to convert the recorded time-domain signal into a mass/charge spectrum.[35] Although the radial and angular frequencies are also mass-dependent, the axial frequency is used because it alone is, to first order, completely independent of energy and of the spatial spread of the ions. High-performance mass analysis, in terms of mass resolution and mass accuracy, can be achieved in the Orbitrap mass analyzer because of this energy independence. Advantages of the Orbitrap include high mass resolution, up to 150000 a result of the fact that the field may be defined with very high accuracy, the increased space charge capacity at higher masses due to independence of trapping potential on mass/charge ratio, and the larger trapping volume compared to FT-ICR and Paul traps. A more subtle point is the concomitant achievement of high mass accuracy, large dynamic range, and a high mass/charge range.

Comparison of Eqns 2 and 4 shows the obvious similarity between the Orbitrap and the QIT, namely, that both electric potential distributions contain a quadrupole component. However, this is a superficial comparison and ignores the important distinction between the two devices, that the QIT is a radio frequency (RF) device while the Orbitrap operates with electrostatic fields (ignoring the initial electrodynamic squeezing used to prepare ions prior to injection into the Orbitrap). Nonetheless, as Guan and Marshall point out in their recapitulation[36] of Major and Dehmelt's pseudopotential treatment,[37] ion axial motion can be reasonably well-approximated as an harmonic oscillator at the ion axial secular frequency (q_z) for $q_z < 0.4$ and by neglecting ion micromotion at higher frequencies. It is now clear that the real similarity between the two devices is that ion motion in the axial direction occurs in an harmonic potential.

DESCRIPTION OF THE MAJOR COMPONENTS OF AN ORBITRAP MASS SPECTROMETER

The Orbitrap mass analyzer forms part of an instrument that was developed and built by Thermo Masslab Ltd (Manchester, UK). Its main components are illustrated in Fig. 2. What follows is a simplified account of ion injection into the Orbitrap mass spectrometer. Readers seeking more detailed accounts may consult previous descriptions[32,33] and the next section. An electrospray source creates ions, which are transferred using an RF-only guide quadrupole (Q_0,
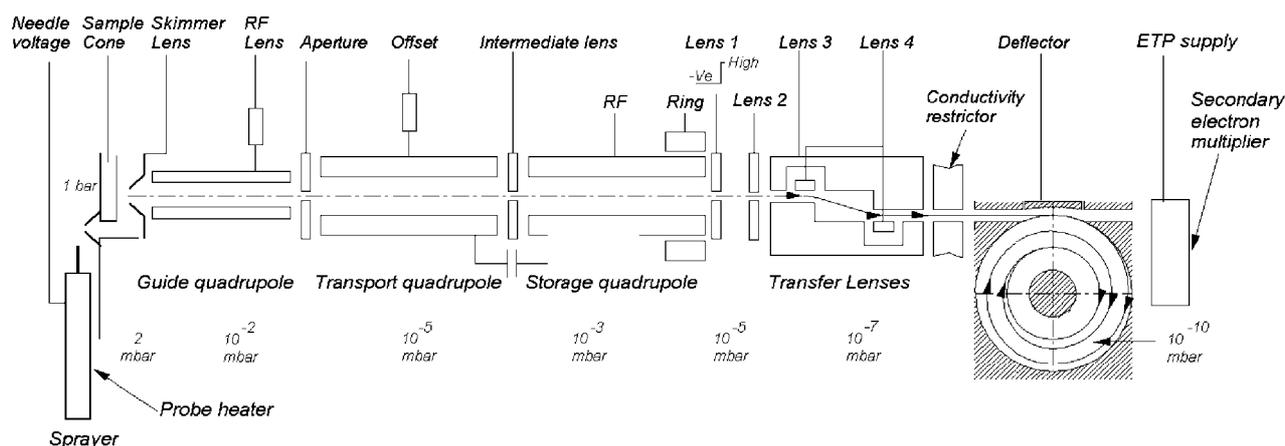
Figure 2. The experimental Orbitrap mass spectrometer. Ions are produced by the electrospray ion source at the extreme left. Ions then proceed through the source, collision quadrupole, selection quadrupole and then pass into the storage quadrupole. The storage quadrupole serves as an ion accumulator and buncher, allowing a pulsed mass analyzer such as the Orbitrap to be coupled to a continuous source like an electrospray ionization source. After accumulation and bunching in the storage quadrupole, the exit lens ('Lens 1') is pulsed low, the ion bunches traverse the ion transfer lens system and are injected into the Orbitrap mass analyzer (shown end-on).

2.5 MHz, $V_{op} = 0.1–1$ kV) into a transport quadrupole (Q_1, 920 kHz, $V_{op} = \sim300$ V). These two quadrupoles bring the ions through several stages of differential pumping from the atmospheric pressure ion source. The ions then proceed into a linear quadrupole ion trap (linear Paul trap, Q_2, 3.45 MHz, $V_{op} = 3700$ V) or 'storage quadrupole'. The storage quadrupole is required to couple the continuous electrospray ion source with the Orbitrap, which operates in a pulsed fashion.

A ring placed over the end of the storage quadrupole rods can be biased by a DC offset, thereby creating a small axial potential well inside the storage quadrupole. Ions suffer just enough collisions with the bath gas ($\sim10^{-4}$ Torr) to cause them to slow down and 'pool' in the axial well as packets of ions of small spatial extent (few mm). After a sufficient number of ions has been accumulated (typically taking 10–400 ms), the back lens of the storage quadrupole is pulsed open. This creates a strong electric field along the axis of the storage quadrupole, causing rapid extraction of the pooled ions, and delivering ion packets with remarkably small temporal (100–200 ns) and spatial spread at the entrance to the Orbitrap.[33,38] Ions are accelerated through an ion optical deflection lens system and delivered to the entrance channel. Injection of ions into the Orbitrap analyzer is accomplished by switching the voltage applied to the deflector lens located on the Orbitrap circumference to an appropriate value.

Once injected into the Orbitrap at a position offset from its equator ($z = 0$), these ion bunches start coherent axial oscillations without the need for any additional excitation. All ions have exactly the same amplitude, although ion packets of different mass/charge ratios will execute their axial oscillations at their respective frequencies, as given by Eqn. 5. The detection of an ion image current due to motion along the Orbitrap axis is only possible so long as the ion packets retain their spatial coherence (viz., phase coherence and small spatial extent) in the axial direction.[32] The outer electrode is split in half at $z = 0$, allowing the ion image current due to axial motion to be collected. The current is differentially amplified from each half of the outer electrode and then undergoes analog-to-digital conversion before processing and collection by customized control and acquisition software (Orbitrap Tune Program, Mike Senko, Thermo Electron, San Jose, CA). Further processing is done by the MIDAS data analysis program.[34] The Orbitrap used for these experiments is smaller than those used in previous experiments.[32,33] The largest diameter of the inner electrode is 8 mm; the largest diameter of the inner surface of the outer electrode is 20 mm.

Data are collected for up to 1600 ms, after an initial delay of ~100 ms to allow sufficient time for the stabilization of the high-voltage amplifier supplying the voltage to the central electrode. The acquired time-domain signal takes the form of a 'transient'. An example of the transient used to record a spectrum showing the 5+, 4+, and 3+ ions of bovine insulin appears in Fig. 3. Ion collisions with background gas molecules, even at the ultra high vacuum levels in the Orbitrap (2×10^{-10} mbar), result in ion packet dephasing (loss of phase coherence), or ion loss from the trap, or both, eventually causing a decrease in the signal intensity of the transient. Space charge may also play a small role in ion packet dephasing. The transient is then Fourier-transformed using the program MIDAS[34] to create a mass spectrum (see the following text for examples).

ION MOTION IN THE ORBITRAP INSTRUMENT

Preparation of the ion packet

Capture of ions by the gas-filled storage quadrupole proceeds in a manner similar to that which occurs in other linear traps.[39,40] Ions enter the storage quadrupole and lose their energy in collisions with gas molecules, thereby becoming unable to escape. One of the novel features of this setup relative to previous experiments[33] is the ability to maintain both the ion source and the Orbitrap at near-ground potential while at the same time accelerating ions to >1 keV in

(a)

Expansion Plot

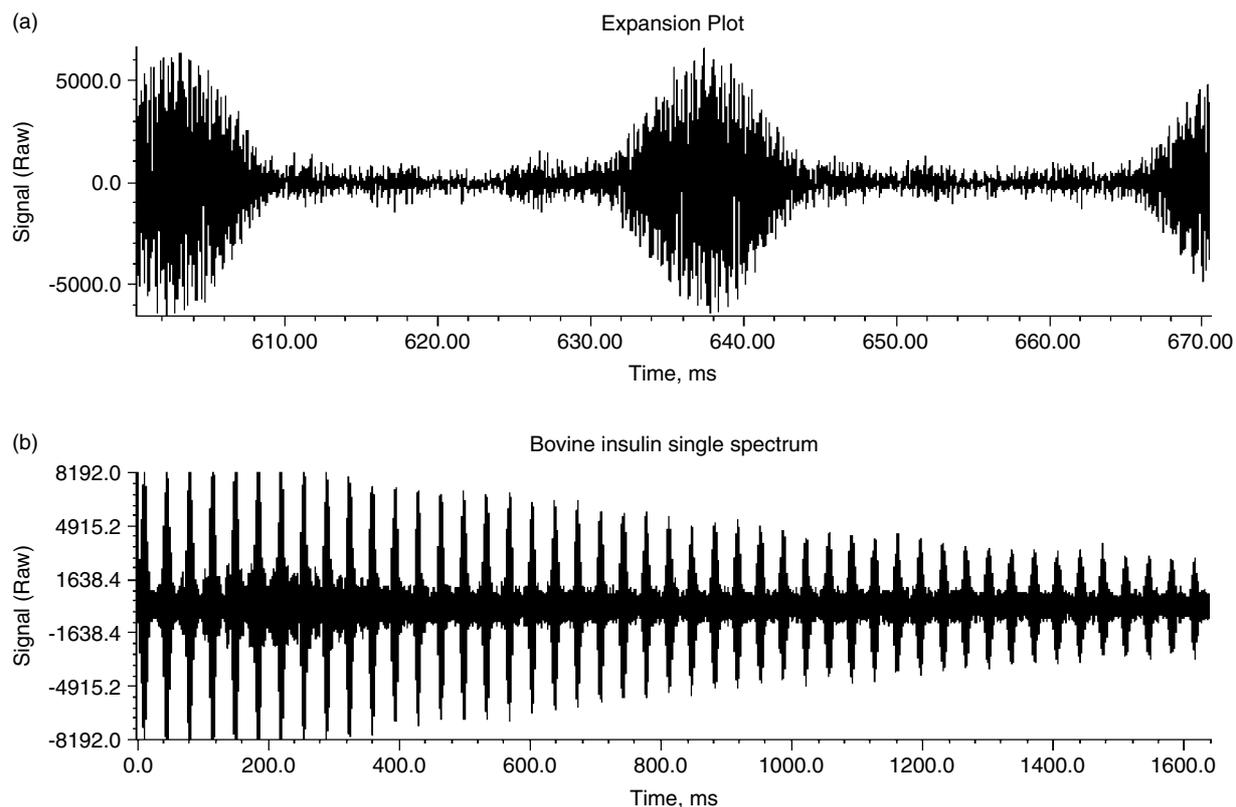(b)

Bovine insulin single spectrum

Figure 3. (a) Typical transient acquired to record the mass spectrum of bovine insulin. The transient acquired is equivalent to the free induction decay of FT NMR experiments. Top shows an expanded portion of the transient.
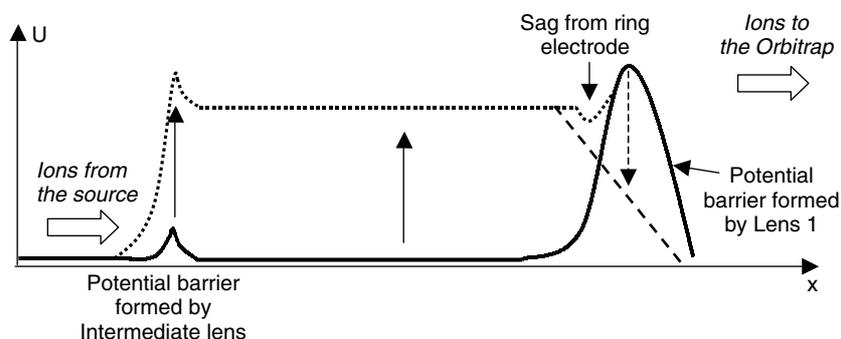

Figure 4. Schematic of energy lift of the storage quadrupole. Axial voltage distribution during ion capture is denoted by the solid line and after the energy lift by the dotted line. For ion extraction, the voltage on Lens 1 is pulsed down forming the voltage distribution indicated by the dashed line.

between. This is achieved by using a so-called 'energy lift' illustrated in Fig. 4. Its operation is based on the fact that while ions are stored inside the storage quadrupole, they stay 'unaware' of outside voltages. Therefore, a slow (over 20–50 ms) and synchronous increase of the DC offset of the storage quadrupole and the intermediate lens voltage does not affect ion trapping as long as ions are still being repelled by the high voltage applied on Lens 1. After Lens 1 is pulsed open, ions are able to 'roll down' from the new level towards the Orbitrap at near-ground potential, thus acquiring the necessary energy for ion injection and orbital trapping.

Another distinctive feature of this setup is the use of a static voltage on the ring electrode to form a miniature potential well near the exit of the storage quadrupole. With thin edges of the ring electrode protruding prominently

between the round rods of the storage quadrupole, any voltage difference between the ring and the rods results in a 3D potential distribution being added to the overall quadrupolar field. When the DC offset of the storage quadrupole exceeds the voltage on the ring electrode, this 3D potential distribution leads to a localized potential well along the axis of the storage quadrupole, the maximum axial sag being approximately equal to 1% of the voltage difference (up to 10–15 V in the current setup). This potential well appears and deepens in the later stages of energy lift, becoming the lowest point on the potential energy surface seen by the ions. In the presence of collision gas, ions tend to concentrate near the bottom of this potential well while they remain confined radially by the RF field applied to the rods. In the last moments before

extraction, ions form dense and compact packets, as in Paul traps.

Ion extraction and transport to the Orbitrap

Pulsed extraction of ions follows the earlier description.[33] Stored ions are extracted by supplying a negative voltage pulse to Lens 1 (Fig.2). Lens 1 also forms a differential pumping aperture, while the length of the ion path from the initial location in the potential well to the exit from Lens 1 within the gas-filled storage quadrupole does not exceed 5–8 mm. Therefore, the probability of collisions and collision-induced dissociation during ion extraction is relatively low. Further lenses perform the final spatial focusing of the ion beam into the entrance of the Orbitrap. Lens 3 also produces a reduction of gas load by eliminating direct gas transport. The latter effect relates to the collision-free penetration of residual gas molecules from the storage quadrupole into the Orbitrap along the line of sight. At the short distances employed, this effect might have easily become the main source of ion scattering inside the Orbitrap. This effect is eliminated by directing the ion beam along an S-shaped path between two symmetrical deflectors, thereby blocking the line of sight.

Ion capture and squeezing in the Orbitrap

Because of the fast pulsing of ions from the storage quadrupole, ions of each mass/charge ratio arrive at the entrance of the Orbitrap as short packets only few millimeters long. For each mass/charge population, this corresponds to a spread of flight times of only a few hundred nanoseconds for mass/charge ratios of a few hundred Daltons/charge. Such durations are considerably shorter than a half-period of axial ion oscillation in the trap. When ions are injected into the Orbitrap at a position offset from its equator (Fig. 5), these packets start coherent axial oscillations without the need for any additional excitation.

Linear quadrupole ion traps have been used for ion packet injection into quadrupole ion traps,[41] Fourier transform-ion cyclotron resonance,[42] and time-of-flight mass spectrometers,[43] and three-dimensional quadrupole ion traps have been used to inject ions into ion mobility spectrometers;[44] however, ion packets in all these examples are 2–3 orders of magnitude longer even for a single m/z, and extraction and injection processes are much slower. The closest analog to fast injection into the Orbitrap is offered
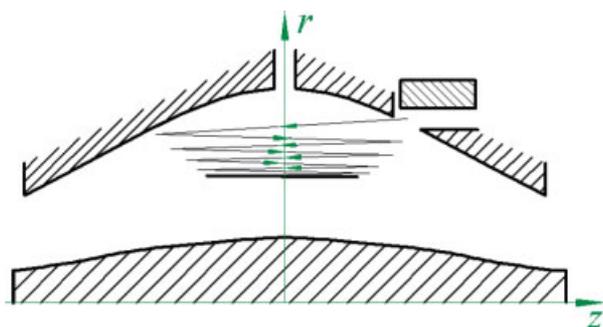

Figure 5. Principle of electrodynamic squeezing of ions in the orbitrap as the field strength is increased.

by 3D quadrupole ion traps, when used to inject ions in-line into time-of-flight mass spectrometers.[45]

Evolution of ion packet during the increase of electric field is shown schematically on Fig. 5. By the time injected ions approach the opposite electrode for the first time, the increased electric field contracts the radius of the ion cloud by a few percent, the voltages having been so chosen to avoid collision with the electrode. A further increase of the field continues to squeeze the trajectory closer to the axis, meanwhile allowing for newly arriving ions (normally, with higher m/z) to enter the trap as well. After ions of all m/z values of interest have entered the Orbitrap and moved far enough from the outer electrodes, the voltage on the central electrode is stabilized, and image current detection may take place. The rise-time of the field strength is selected depending on the mass range to be trapped and is usually within 20–100 µs.

It should be noted that squeezing affects both radial and axial amplitudes of ions. Because of the difference in moments of injection into the Orbitrap for ions of different m/z, this results in slightly different final amplitudes of rotation and axial oscillation.

Rotational motion and ion trapping

The rotational (r, φ) motion, although not used for mass analysis, is still important because the ions must be trapped radially. This motion, and its relationship to the ion kinetic energy, can be crudely understood if the Orbitrap is regarded as a '360° electrostatic analyzer'. In any electrostatic sector, ion motion along a circular trajectory is described by the equation[46]

$$r = 2\,eV/eE \qquad (6)$$

where r is the radius of the electrostatic analyzer as well as the radius of the ion trajectory through the analyzer, eV is the ion's kinetic energy, and eE is the force due to the electric field (directed radially inward) experienced by the ion while traveling on the ion-optical axis. This equation is derived by balancing centrifugal and centripetal forces acting on the ion.[46] Significantly, Eqn. 6 is independent of mass. The electric sector selects for ion kinetic energy provided that the sector radius, r_E, is fixed, because when the strength of the electric field is set to a particular value, only ions of the appropriate energy, as given by Eqn. 6, will be transmitted through the sector.

Similarly, ion kinetic energy before injection into the Orbitrap must be suitably matched to the radial component of the electric field to result in stable orbital motion. Makarov has shown that stable ion motion results from nearly circular orbits with very small eccentricities.[32] In a sense, every orbit around the Orbitrap central electrode 'analyzes' the kinetic energy of the ion. This situation is somewhat analogous to the Osaka MULTUM II TOF instrument. This instrument consists of four 157.1° electric sectors in a 'cloverleaf' arrangement, allowing an arbitrary number of cycles through the sectors to be used to achieve the desired performance (e.g. resolution).[47–49]

Figure 6 depicts the Orbitrap functioning as a 360° analyzer using SIMION simulations.[50] Orbits are at constant

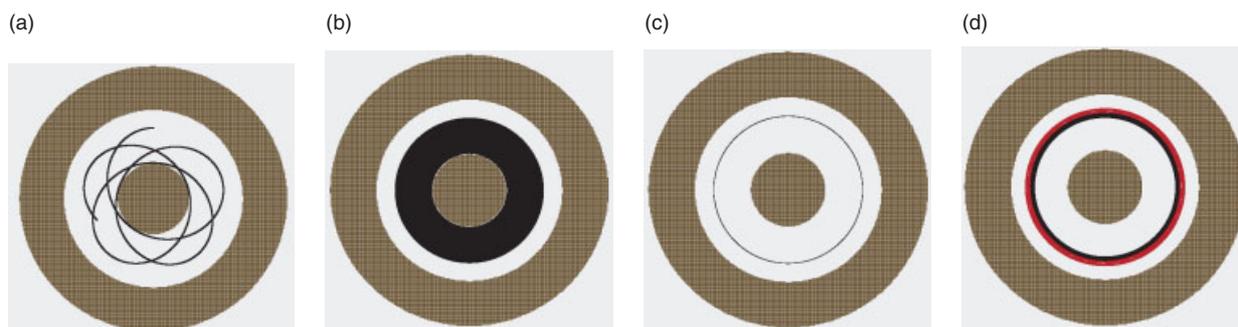(a)   (b)   (c)   (d)

Figure 6. Matching of incoming ion kinetic energy to the radial component of the Orbitrap electric potential. Ion trajectories are shown for $z = 0$. (a) Incoming ion kinetic energy poorly matched to the radial component of the electric field, resulting in a highly eccentric, non-circular orbit. A few periods of the orbit, showing the rapid precession of perigee, are shown. (Trajectory trace line thickened to aid visibility). (b) Same incoming ion kinetic energy as in (a) but with hundreds of periods shown. Because of the large eccentricity and precession of the orbit, the locus of orbits appears as a 'fat doughnut'. (c) Ion kinetic energy (1620 eV) well matched to radial component of the electric field. This orbit is nearly circular, resulting in a locus of orbits that appears as a thin ring. Thousands of periods are shown superimposed and a thin trajectory trace line used. (d) Locus of orbits of two ion kinetic energies, 1570 and 1670 eV. Nearly circular orbits demonstrate the kinetic energy acceptance range of the Orbitrap.

axial position, $z = 0$, for singly charged ions of mass 609 Da. The central electrode is set at −3400 V. Figure 6a shows the first few orbits of an ion with kinetic energy 930 eV, a value that is poorly matched to the radial field. The orbit is highly elliptical, with the perigee (point of closest approach to the central electrode) precessing very rapidly. Figure 6b shows the same ion, but in an integrated view after hundreds of orbits, so that the accumulated orbits appear collectively as a fat doughnut surrounding the inner electrode. Figure 6c shows another ion whose kinetic energy, 1620 eV, is now well matched to the central electrode voltage. Figure 6c shows 10–100 times more orbits than Fig. 6b, but 6c retains the appearance of a 'thin ring' because the ion kinetic energy is now matched to the 'pass' energy of the trap. The result is nearly circular orbit trajectories, varying little from orbit to orbit, which fall atop one another. Figure 6d shows the loci of orbits for ions of the two kinetic energies of 1570 and 1620 eV. Although clearly the orbits are not circular, they still have relatively small eccentricities, showing that the Orbitrap will be relatively tolerant of a range of incoming ion kinetic energies. The fact that ions with a kinetic energy distribution have different orbits in the Orbitrap makes for a larger trapping volume and therefore increases space charge capacity.

Axial ion motion and ion detection

During ion detection, both the central electrode and deflector are maintained at very stable voltages so that no mass drift can take place. The voltage on the deflector is switched to a level that minimizes 'field sag' caused by the injection slot. This is necessary to ensure that all ions experience the harmonic axial potential in all parts of space, thereby minimizing differences in frequency for ions of a given m/z value.

As mentioned previously, stable ion trajectories within the Orbitrap combine axial oscillations with rotation around the central electrode and vibrations in the radial direction (Fig. 1). For ions of any given m/z, only the frequency of axial oscillations is completely independent of initial ion
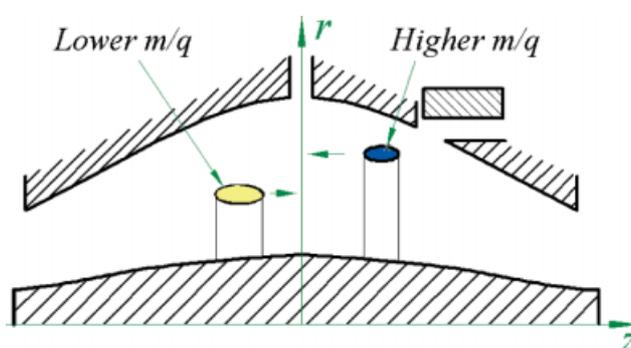

Figure 7. The approximate shape of ion packets of different m/z after stabilization of voltages. The Orbitrap is shown in cross-section along the z-axis. Ovals represent cross sections for thin rings of ions of different m/z. The cross-sectional area is exaggerated for illustration purposes.

parameters,[32] while rotational and radial frequencies exhibit strong dependence on initial radius and energy. Therefore, ions of the same mass/charge ratio continue to oscillate along z together, remaining in-phase for tens and hundreds of thousands of oscillations. Contrary to this, the frequencies of radial and rotational motion will vary for ions with slightly different initial parameters, which means that in the radial direction, ions dephase orders of magnitude faster than in the axial direction, and the process occurs in a period of only 50–100 oscillations. After radial dephasing, the ion packet of a given m/z (and kinetic energy) assumes the shape of a thin ring, with ions uniformly distributed along its circumference (Fig. 7). Consequently, opposite sections of this ring produce opposite image currents on the outer electrodes that ultimately cancel each other out. Therefore, radial and rotational frequencies cannot appear in the measured spectrum in any form. Meanwhile, axial oscillations will persist, with axial thickness of the ion ring remaining small compared with the axial amplitude. Moving from one half outer electrode to the other, this ring will induce opposite currents on these halves, thus creating a signal that is detected by differential amplification.

Though initially small, the axial thickness of the ion ring will grow very slowly because of miniscule imperfections of the Orbitrap shape. Also, ion collisions with background gas molecules, even at the ultra high vacuum levels in the Orbitrap (2×10^{-10} mbar), result in the loss of some ions, or at least displace them outside the initial ring. Space charge may also play a small role in mutual repulsion of ions within the ring and therefore in ion packet broadening. Ultimately, all these factors will result in the ion ring's axial thickness becoming comparable with the amplitude of the axial oscillations. Then, as for radial or rotational motion, image currents due to different parts of the ion ring will start to cancel each other out, thus reducing the intensity of the signal until it is completely lost in the noise.

RESULTS

Performance characteristics

Performance parameters used to characterize a mass spectrometer include resolution, mass accuracy, mass range or upper mass limit, and ion dynamic range.[8] Perhaps the most striking aspect of the Orbitrap's performance is the very high resolution obtained. For example, the electrospray ionization source (ESI) mass spectrum of bovine insulin is shown in Fig. 8. The main spectrum shows the mass region from m/z 1000 to 2200. In addition to the prominent peaks due to the three charge states of +3, +4, and +5, peaks due to Ultramark oligomers, used as internal mass calibrants,[51] are visible, spaced by 100 mass/charge units. Close-ups above

the full spectrum display both the theoretically expected[46] (upper traces, IsoPro 3.0, MS/MS Software[52]) and the experimental isotopic distributions (lower traces) for each of the charge states. Agreement between the experimental and theoretical distributions is reasonably good.

As another example of the resolution obtainable, Fig. 9 presents the mass spectrum of the tetrapeptide Met-Arg-Phe-Ala (MRFA). The mass spectrum shows the main isotopic peak at $m/z = 524$, with the first and second isotopic peaks at 525 and 526. The inset shows a close-up of the second isotope peak at m/z 526, and its resolution into two minority isotopomers ($^{13}C_2$ and ^{34}S). The difference of m/z 0.0109 between these two isotopomers requires a minimum resolving power of 48 300. This high resolving power and ability to distinguish minor isotopes, coupled with high-mass accuracy, may greatly assist in determining chemical formulas for peptides and other species.

Another important performance characteristic of a mass analyzer is the upper mass limit. Shown in Fig. 10 is the nanospray mass spectrum of baker's yeast (*Saccharomyces cerevisiae*) alcohol dehydrogenase (ADH). Though not of high quality, the spectrum compares favorably with those recorded using other types of mass spectrometers. The peaks correspond to the +28, +27, +26, and +25 charge states of ADH tetramers.[53,54] The mass spectrum shows the current upper mass range for this instrument, albeit without the high resolution normally obtained at lower masses. The limitation in mass range at this point is most likely due
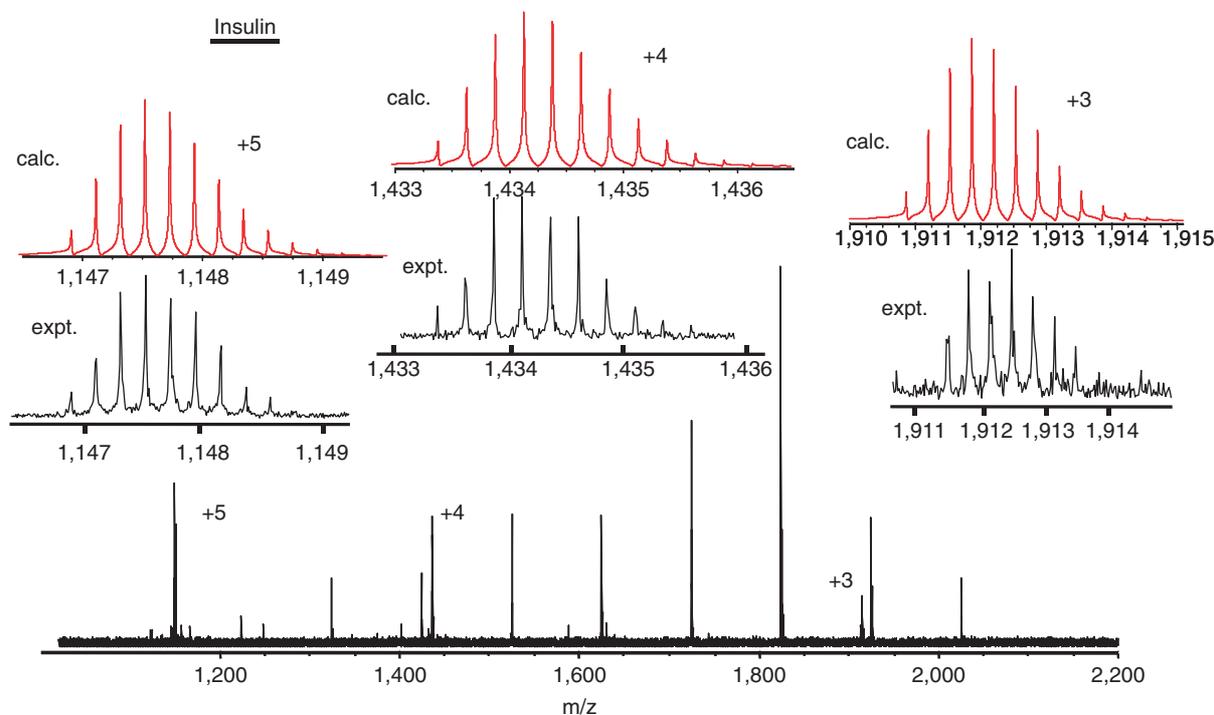

Figure 8. ESI mass spectrum of bovine insulin. Data acquisition parameters include a data sampling rate of 5 MHz, record length was 8 million data points, and the Fourier transform was performed with no apodization function or zero-filling. The lower spectrum shows a wide range mass spectrum including the internal mass calibrant Ultramark 1621 whose oligomers are spaced by 100 mass/charge unit intervals. Lower traces in the close-ups show experimentally obtained isotopic distributions for each charge state. Upper traces in the close-ups show the theoretically expected isotopic distributions. The calculated isotope distributions were obtained from IsoPro 3.0 using Gussian peak shapes with resolution of 100 000.
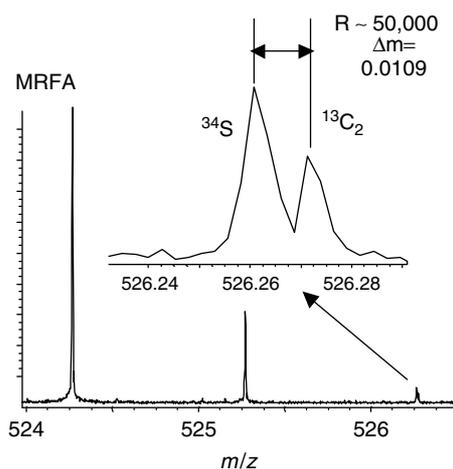
Figure 9. ESI mass spectrum of the singly protonated tetrapeptide MRFA. The inset shows the resolution of the two minority isotopomers at nominal *m/z* 526. The minor isotope ^{34}S is at *m/z* 526.2607, while the higher mass isotope corresponding to ^{13}C$_2$ is at *m/z* 526.2716, a mass difference of *m/z* 0.0109. The minimum resolving power needed to resolve these peaks is 48 300.
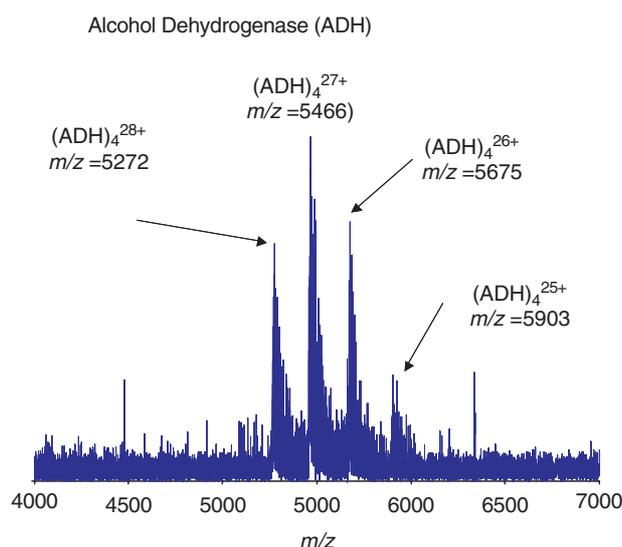

Figure 10. Nanospray mass spectrum of alcohol dehydrogenase (ADH) showing performance at high mass/charge ratio.

to poor high-mass transmission in the double orthogonal geometry ion source rather than a limitation of the Orbitrap mass analyzer. Poor high-mass transmission in the source at least partly accounts for the relatively poor signal/noise ratio of this mass spectrum.

Mass measurement accuracies of 10 ppm or better can provide useful information about possible analyte molecular formulas. The mass accuracy of the Orbitrap was assessed by making measurements of poly(ethylene glycol) oligomers. The oligomer at *m/z* 1075.648 was used as the internal mass calibration standard. Over the *m/z* range of 700 to 1200, the average root-mean-square (RMS) deviation (theoretical mass vs experimentally measured mass) was 2.1 ppm while the mean deviation was 1.7 ppm for a series

of five measurements. This result is robust; similar results were obtained on repeating this experiment under the same or similar conditions on different occasions. Daily calibration of the instrument was performed using just a single reference ion, either that of reserpine at *m/z* 609 or that of MRFA at *m/z* 541.

Also of interest is the mass accuracy observed for the insulin mass spectrum shown in Fig. 8. Use of the ultramark oligomers as mass calibrants using a linear calibration over the range *m/z* 1121–2021 yielded an average RMS uncertainty in the insulin masses (all isotopomers) of 2.9 ppm for the +5 charge state centered at *m/z* 1149, 1.5 ppm for the +4 charge state at 1436, and 4.9 ppm for +3 at 1915.[55] The larger deviation for the +3 charge state may be due partly to its poor signal/noise characteristics. However, much better agreement is achieved if a linear calibration is constructed using the lowest *m/z* insulin isotopomer in the +5 charge state distribution (theoretical *m/z* 1148.491) and the highest *m/z* isotopomer observed in the +4 charge state (*m/z* 1437.529). In that case, the RMS deviation becomes 0.6 ppm for the +5 and 0.9 ppm for the +4 distribution.

The dynamic range has also been measured for the Orbitrap as a function of analyte (reserpine) concentration. The linear dynamic range is roughly 10^3–10^4, corresponding to 0.5 to 500 ng/μL using a particular electrospray ion source (150 °C, 3000 V, 5 μL/min) and instrument parameters (fixed 70 ms accumulation time in the storage quadrupole). This compares favorably with both quadrupole ion traps, with dynamic ranges between 10^2 and 10^3, strongly depending upon the number of ions present (space charge),[8] and with recently reported work on an FT-ICR 3 Tesla analyzer coupled to a linear ion trap that found a range of 10^3–10^4.[56] We note that no special arrangement was made to eject matrix ions from the storage quadrupole and that the dynamic range might be limited by the storage quadrupole and the accumulated chemical noise therein, rather than by the Orbitrap.

Applications

The Orbitrap has been applied to a number of chemical systems, chosen because they provide tests of instrument performance as well as being of scientific interest. Some of the most interesting results have been obtained in studying the serine octamer. Very briefly, serine octamer has been observed under electrospray conditions to form the magic number cluster Ser$_8$H$^+$ and related metacluster ions. Conditions can be found in both a quadrupole ion trap instrument (LCQ instrument, ThermoFinnigan)[57,58] and a triple quadrupole instrument[59] where they are nearly the exclusive ions obtained in the mass spectrum. Even more intriguingly, through labeling studies and by electrospraying combinations of L and D serine, it has been demonstrated that the octamer preferentially forms from one enatiomer, that is, it is homochiral. The serine cluster is especially interesting because it has been argued[57] that it might have played a role in homochirogenesis—the process in which a single, preferred chirality was selected and transmitted to all biological molecules in the early pre-biotic earth. For example, on earth all biologically synthesized amino

acids have L-configurations, whereas all sugars have D-configurations. The possible role of serine and serine clusters in this process is suggested by the observation of reactions between serine octamers and various biological molecules, such as the preferential formation of mixed L-serine/D-glucose clusters under electrospray conditions from solutions containing both L- and D-glucose.[60]

One area of interest is whether the metaclusters, most notably $(Ser_8H)_2^{2+}$ and $(Ser_8H)_3^{3+}$, also contribute to the observed serine octamer peak.[58] Of course, the monoisotopic mass peak for these species will have the same mass/charge ratio as the regular octamer. However, the ^{13}C-substituted isotopomers of the metaclusters will have different m/z ratios and thus will be separately observable given sufficient resolution. So, for example, the $^{13}C_1$-isotopomer of $(Ser_8H)_3^{3+}$ has a mass/charge ratio 1/3 unit higher than the monoisotopic peak. Such a peak is observable in the Orbitrap with its higher resolution, but not in a quadrupole ion trap instrument. Figure 11 shows the resulting mass spectrum, with peaks due to the $^{13}C_1$, $^{13}C_2$ and $^{13}C_4$ isotopomers of $(Ser_8H)_3^{3+}$ and the $^{13}C_1$ isotopomer of $(Ser_8H)_2^{2+}$ clearly visible; $^{13}C_3$-$(Ser_8H)_3^{3+}$ is coincident with $^{13}C_1$-Ser_8H^+. Although indirect evidence for the metaclusters was obtained with the quadrupole ion trap, this mass spectrum is the first direct observation of the metaclusters.

Previous research[58] strongly suggested that the protonated serine metaclusters were relatively unstable. Studies in the Orbitrap instrument confirm the relative instability of the protonated metaclusters. Figure 11 shows the mass spectrum recorded in the Orbitrap instrument by electrospraying a 0.01 M L-serine solution (in methanol/water/acetic acid 50 : 49 : 1 v/v) at a nitrogen pressure of 3.8×10^{-3} mbar inside the storage quadrupole. Increasing the pressure to 7×10^{-3} mbar causes the disappearance of the metacluster peaks, while the intensity of the protonated serine octamer does not change appreciably, confirming both the findings of relatively fragile metaclusters and of the exceptional stability of the serine octamer. Destruction of the serine octamer metaclusters most likely occurs in the storage quadrupole, as the Orbitrap pressure remains virtually constant while pressure is changed in the storage quadrupole.

The structure of the serine octamer has also been a topic of interest in the literature. Serine-dimer losses from the protonated octamer are predominant in MS^2 and MS^3 experiments,[57,61] leading to the proposal that a quartet of neutral serine dimers comprises the octamer structure.[57] On the basis of the ion mobility data and *ab initio* calculations, other structural types have also been suggested, some made up of zwitterionic monomers.[61–63] The fundamental distinction between these two structures is whether the individual serine molecules are present in the octameric cluster in the neutral form or in the charge separated zwitterionic form. These considerations also suggest that the serine octamer might have at least two possible conformers. In the 'neutral form' conformer, all the serine molecules are held together by hydrogen bonding forces. In the 'zwitterionic form' conformer, all the serine molecules all held together by ionic forces as well as by hydrogen bonding. Intuitively, the 'zwitterionic form' conformer is expected to have a much more compact structure than the 'neutral form' conformer due to the stronger ionic binding forces.

Ion/molecule reactions can be used to probe gas-phase ion structures. For example, gas-phase hydrogen/deuterium (H/D) exchange has been successfully applied to obtain structural information on various types of molecules from singly charged small ions to large multiply charged protein ions, especially in distinguishing isomeric ions and identifying conformer structures of proteins and peptides.[64–67] In H/D exchange reactions, the exchangeable protons in the ion of interest are replaced by deuterium present in the neutral reagent gas. The H/D exchange rate is controlled by the types of exchangeable protons (amine, alcohol, carboxyl etc.), the presence of intramolecular interactions (hydrogen bonding, ionic forces etc.), steric factors, and the number of collisions. Therefore, H/D exchange can provide insights into the roles of non-covalent interactions and the resulting ion structure in gas-phase ions. H/D exchange of amino acids, primary alcohols, peptides, and nucleotides, as well as the role of zwitterionic structures and internal salt-bridges, has been studied in detail.[66–72]

H/D exchange of the serine cluster ions was carried out in the storage quadrupole, where CH_3OD was introduced at a pressure of 5×10^{-3} mbar as the H/D exchange reagent. The
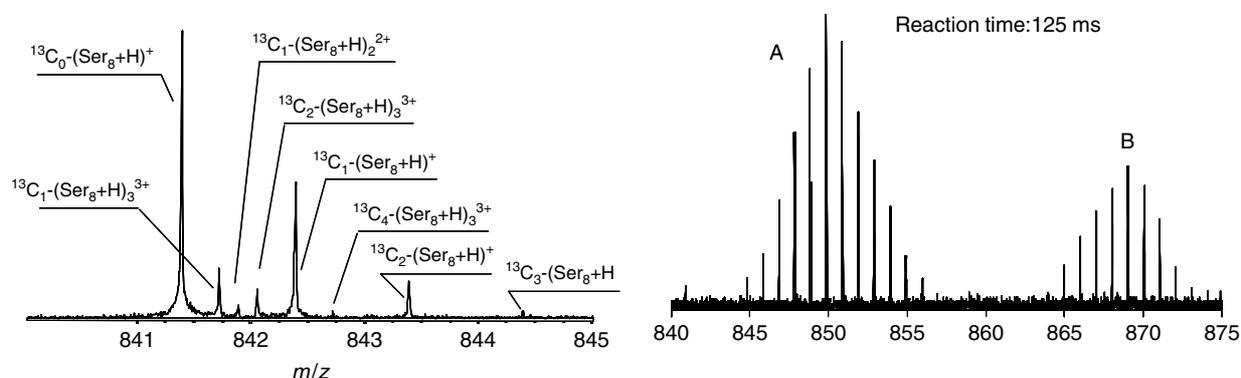

Figure 11. Serine octamer mass spectra. (a) Serine octamer peak and peaks due to clusters of the octamer ('metaclusters') showing ability to examine non-covalent clusters in the Orbitrap using ESI (0.01 M L-serine in methanol/water/acetic acid 50 : 49 : 1 v/v). (b) H/D exchange mass spectrum of serine octamer using CH_3OD. The spectrum shows two populations of serine octamer in the ion beam. Unexchanged octamer has m/z of 841.

Orbitrap was used to characterize the exchange products. This arrangement parallels previous work where CID was performed in the storage quadrupole.[73] The reaction time (120–5000 ms) was varied by changing the ion residence time in the storage quadrupole prior to injection into the Orbitrap. Figure 11b shows the H/D exchange reaction of L-serine (electrospray, 0.01 M in 50/50 methanol/water with 1% acetic acid) at 125 ms reaction time. The octamer possesses 33 exchangeable hydrogen atoms (amine, hydroxy, and acid groups and charge-carrying proton); clusters can appear at m/z ratios between 841 (no exchange) to 874 (complete exchange). The observed bimodal distribution indicates that L-serine octamer has at least two structures. The ions in population B have undergone H/D exchange reaction more readily than ions in population A, judging by the extent of reaction. Mass spectra were also collected at longer reaction times and greater CH_3OD pressures. The distribution of lower mass/charge ratio has moved to higher mass/charge ratios due to the higher rates of reaction at higher CH_3OD pressures and longer times.

These results are consistent with the earlier findings[59] on H/D exchange at atmospheric conditions in both sonic spray and electrospray preparation of serine octamers. The earlier data also showed two populations and population B was assigned to the neutral form, a structure argued to be less tightly bound and therefore more accessible to the H/D exchange reagent. Moreover, its formation was favored under more energetic electrospray conditions (perhaps by fast conversion from conformer A). Population A was assigned to the zwitterionic form. Other workers have confirmed the presence of a second population.[74]

Mass spectra were recorded for a variety of transition metal/ligand complexes, including Zn complexes with histidine, citric acid, malic acid, and 1-methyl histidine, Cd complexes with histidine and 1-methyl histidine, and Ni complexes with phenylalanine.[75] Such complexes are found in metal hyper-accumulating plants, which are under study for phytoremediation of heavy-metal−contaminated sites. Work is ongoing to understand more about their spatial and temporal distributions in these plants.[76] The complexes were formed by electrospraying solutions containing $\sim 10^{-4}$ M metal cation and 5×10^{-4} M organic acid. Typical instrumental conditions included a slightly deeper axial well in the storage quadrupole, which seemed to favor formation or retention of the complexes. As an example, the electrospray mass spectrum of a solution containing 1×10^{-4} M Zn^{2+} (aq) and 5×10^{-4} M histidine (M-His) is shown in Fig. 12. Singly charged zinc/methyl-histidine complexes with ratios of 1:2, 1:3, 2:3, and 3:4 were observed, as well as the protonated methyl-histidine dimer. The figure inset shows the very complicated experimental isotope pattern due to the complex $[Zn_3(MeHis)_4(H_2O)_2]^+$ and its simulation. Observation of the last three isotopomers (m/z 916, 917, and 918) was precluded by the low abundance of this complex and hence poor signal/noise ratio. Similar results were obtained for the other Zn or Cd/ligand systems as well as the Ni/phenylalanine system.

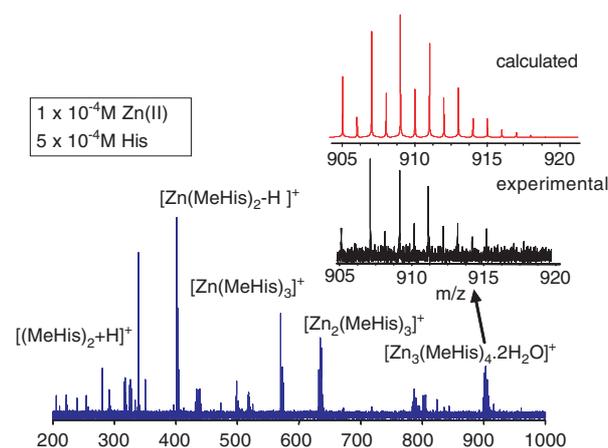Oligosaccharides are also an area of increasing interest,[77,78] especially because of their importance in drugs,

Figure 12. Electrospray mass spectrum of a solution containing 1×10^{-4} M Zn(II) and 5×10^{-4} M 1-methyl-histidine ('M-His'). Inset: comparison of theoretical (top, IsoPro) and experimental (bottom) isotope distributions for the $Zn_3(MeHis)_4(H_2O)_2^+$ complex.
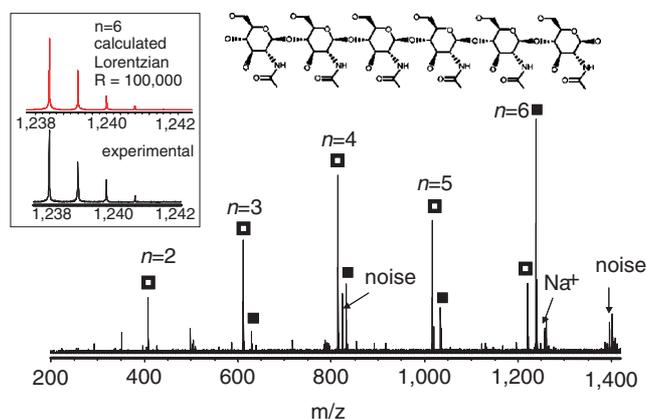

Figure 13. ESI mass spectrum of hexa-*N*-acetyl chitohexaose. Inset shows a close-up of the experimental (lower trace) and theoretically expected (upper trace) isotopic distributions. Filled squares denote ions with structure $[(saccharide)_nOH_3]^+$, while open squares denote fragment ions with structures $[(saccharide)_nH]^+$.

nutrition, and protein/carbohydrate interactions. Figure 13 shows the mass spectrum obtained for the oligosaccharide hexa-*N*-acetyl chitohexaose (structure presented in figure). Singlycharged (protonated) fragment ions corresponding to 2, 3, 4, and 5 saccharide units (denoted by the filled squares in Fig. 13) and their dehydration products (open squares in Fig. 13) were observed, as well as the protonated parent molecule, its dehydration product, and its Na^+ complex. The theoretically expected isotopic distribution for the parent ion compares well with that observed experimentally (Figure inset). Fragmentation might be taking place in either our ESI source or the storage quadrupole (Q_2).

As a final example of an application of the performance of the Orbitrap, Fig. 14 illustrates the ESI mass spectrum of vancomycin, a cyclic glycopeptide. Vancomycin is an important antibiotic, often used as a last resort in serious infections. The mass spectrum shows the protonated parent molecule at m/z 1448 and several fragment ions. Major
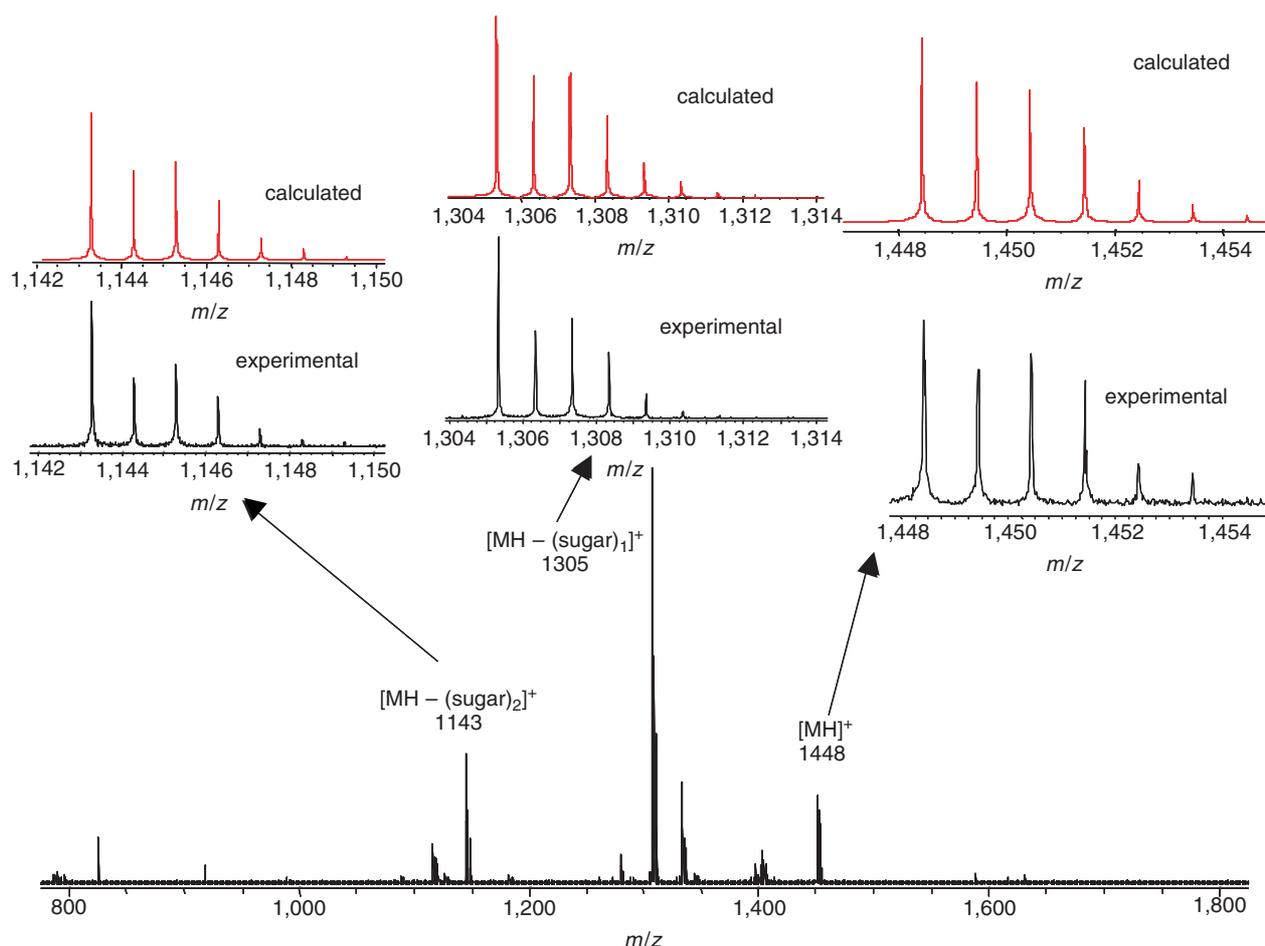
Figure 14. ESI mass spectrum of the antibiotic vancomycin. Insets show experimental (bottom traces) and simulated (IsoPro, top traces) isotopic distributions for parent ion (MH+) and protonated fragment ions corresponding to the loss of one or two sugar moieties. The doubly charged cation at *m/z* 725 was not observed.

fragment ions include m/z 1305, corresponding to the loss of one saccharide; m/z 1277, which corresponds to be the additional loss of CO; m/z 1143, the loss of both sugars units and m/z 1115, which appears to be due to the loss of two sugars and CO. Once again, fragment ions appear in the mass spectrum. Intriguingly, all literature spectra show ESI spectra with no fragmentation and show the doubly charged ion MH_2^{2+} at m/z 725 as the predominant or only ion.[79]

CONCLUSIONS AND FUTURE WORK

The results described here demonstrate that the Orbitrap is a powerful mass spectrometer that can be used to examine a variety of types of chemical systems. It provides high resolution, high-mass accuracy, and good dynamic range. In addition to the examples shown, the instrument has been applied to a wide range of analytes, especially proteins and peptides, oligosaccharides, and glycopeptides. The description provided here of the basis and performance of the instrument is intended as a preparation for more detailed understanding of the unique features of this device. Future work includes designing and fabricating the ion optics necessary for conducting surface induced dissociation as an ion activation method in MS/MS and ion motion control experiments inside the Orbitrap. Simulations of ion

motion in the Orbitrap are also contributing to an improved understanding of its performance and suggesting new types of experiments.

Acknowledgements

REFERENCES

1. Schwartz JC, Wade AP, Enke CG, Cooks RG. Systematic delineation of scan modes in multidimensional mass spectrometry. *Anal. Chem.* 1990; **62**: 1809.
2. Chen H, Zheng X, Cooks RG. Ketalization of phosphonium ions by 1, 4-dioxane: Selective detection of the chemical warfare agent simulant dmmp in mixtures using ion/molecule reactions. *J. Am. Soc. Mass Spectrom.* 2003; **14**: 182.
3. deHoffmann E. Tandem mass spectrometry: a primer. *J. Mass Spectrom.* 1996; **31**: 129.
4. Reid GE, Shang H, Hogan JM, Lee GU, McLuckey SA. Gas-phase concentration, purification, and identification of whole

proteins from complex mixtures. *J. Am. Chem. Soc.* 2002; **124**: 7353.

5. Woods AS, Huang AYC, Cotter RJ, Pasternack GR, Pardoll DM, Jaffee EM. Simplified high-sensitivity sequencing of a major histocompatibility complex class i-associated immunoreactive peptide using matrix-assisted laser-desorption ionization mass-spectrometry. *Anal. Biochem.* 1995; **226**: 15.

6. Bristow AWT, Webb KS. Intercomparison study on accurate mass measurement of small molecules in mass spectrometry. *J. Am. Soc. Mass Spectrom.* 2003; **14**: 1086.

7. Marshall AG, Hendrickson CL, Jackson GS. Fourier transform ion cyclotron resonance mass spectrometry: a primer. *Mass. Spectrom. Rev.* 1998; **17**: 1.

8. McLuckey SA, Wells JM. Mass analysis at the advent of the 21st century. *Chem. Rev.* 2001; **101**: 571.

9. Williams JD, Flanagan M, Lopez L, Fischer S, Miller LA. Using accurate mass electrospray ionization—time-of-flight mass spectrometry with in-source cid to sequence peptide mixtures. *J. Chromatogr., A* 2003; **1020**: 11.

10. Wells JM, Gill LA, Ouyang Z, Patterson GE, Plass W, Badman ER, Amy JW, Cooks RG, Schwartz JC, Stafford GC, Senko MW. Factors affecting the mass measurement accuracy of quadrupole ion trap mass spectrometers. In *Proceedings of the 46th ASMS Conference on Mass Spectrometry and Allied Topics*, Orlando, 1998; 485.

11. Grayson M (ed). *Measuring Mass—From Positive Rays to Proteins*. Chemical Heritage Press: Philadelphia, 2002.

12. Edmond H, Jean C, Vincent S. *Mass Spectrometry Principles and Applications*. Johan Wiley & Sons: New York, 1996; 41.

13. Mattauch J, Herzog R. Mass spectrograph. *Z. Physik* 1934; **89**: 786.

14. Johnson EG, Nier AO. Angular aberrations in sector shaped electromagnetic lenses for focusing beams of charged particles. *Phys. Rev* 1953; **91**: 10.

15. Dawson PH (ed). *Quadrupole Mass Spectrometry and its Applications*. Elsevier Scientific Publishing: New York, 1976; 349.

16. Comisarow MB, Marshall AG. The early development of fourier transform ion cyclotron resonance (ft-icr) spectroscopy. *J. Mass Spectrom.* 1996; **31**: 838.

17. Amster IJ. Fourier transform mass spectrometry. *J. Mass Spectrom.* 1996; **31**: 1325.

18. March R. An introduction to quadrupole ion trap mass spectrometry. *J. Mass Spectrom.* 1997; **32**: 351.

19. Wiley WC, McLaren IH. Time of flight mass spectrometer with improved resolution. *Rev. Sci. Instrum.* 1955; **26**: 1150.

20. Guilhaus M. Principles and instrumentation in time-of-flight mass spectrometry. *J. Mass Spectrom.* 1995; **30**: 1519.

21. Kingdon KH. A method for the neutralization of electron space charge by positive ionization at very low gas pressures. *Phys. Rev.* 1923; **21**: 408.

22. Brooks PR, Herschbach DR. Kingdon cage as a molecular beam detector. *Rev. Sci. Instrum.* 1964; **35**: 1528.

23. Douglass RA, Zabritski J, Herb RG. An orbitron vacuum pump. *Rev. Sci. Instrum.* 1965; **36**: 1.

24. Yang L, Church DA. Confinement of injected beam ions in a kingdon trap. *Nucl. Instrum. Methods Phys. Res., Sect. B* 1991; **B56-B57**: 1185.

25. Lewis RR. Motion of ions in the kingdon trap. *J. Appl. Phys.* 1982; **53**: 3975.

26. Knight RD. Storage of ions from laser-produced plasmas. *Appl. Phys. Lett.* 1981; **38**: 221.

27. Korsunskii MI, Basakutsa VA. A study of the ion-optical properties of a sector-shaped electrostatic field of the difference type. *Soviet Phys.-Tech. Phys.* 1958; **3**: 1396.

28. Gall LN, Golikov YK, Aleksandrov ML, Pechalina YE, Holin NA. USSR Inventor's Certificate, #1247973, 1986.

29. McIlraith AH. *Nature* 1966; **212**: 1422.

30. Bluemel R. Dynamic kingdon trap. *Phys. Rev. A: At., Mol., Opt. Phys.* 1995; **51**: R30.

31. Makarov A. Mass spectrometer. U.S. Patent 5,886,346 1999.

32. Makarov A. Electrostatic axially harmonic orbital trapping: a high-performance technique of mass analysis. *Anal. Chem.* 2000; **72**: 1156.

33. Hardman M, Makarov A. Interfacing the orbitrap mass analyzer to an electrospray ion source. *Anal. Chem.* 2003; **75**: 1699.

34. Senko MW, Canterbury JD, Guan S, Marshall AG. A high-performance modular data system for fourier transform ion cyclotron resonance mass spectrometry. *Rapid Commun. Mass Spectrom.* 1996; **10**: 1839.

35. Marshall AG, Verdun FR. *Fourier transforms in nmr, optical, and mass spectrometry: a user's handbook*, Elsevier: Amsterdam, 1990; 450.

36. Guan S, Marshall AG. Stored waveform inverse fourier transform axial excitation/ejection for quadrupole ion trap mass spectrometry. *Anal. Chem.* 1993; **65**: 1288.

37. Major FG, Dehmelt HG. Exchange-collision technique for the rf spectroscopy of stored ions. *Phys. Rev.* 1968; **170**: 91.

38. Makarov A, Hardman M, Schwartz J, Senko M. PCT Patent Appl. W002078046, 2002.

39. Schwartz JC, Senko MW, Syka JEP. A two-dimensional quadrupole ion trap mass spectrometer. *J. Am. Soc. Mass Spectrom.* 2002; **13**: 659.

40. Hager JW. A new linear ion trap mass spectrometer. *Rapid Commun. Mass. Spectrom.* 2002; **16**: 512.

41. Cha B, Blades M, Douglas D. An interface with a linear quadrupole ion guide for an electrospray-ion trap mass spectrometer system. *Anal. Chem.* 2000; **72**: 5647.

42. Syka JEP, Bai DL, Stafford GCJ, Horning S, Shabanowitz J, Hunt DF, Marto JA. A linear quadrupole ion trap fourier transform mass spectrometer: a new tool for proteomics. In *Proceedings of the 49th ASMS Conference on Mass Spectrometry and Allied Topics*, Chicago, 2001.

43. Wang Y, Park MA, Giessmann UP, Laukien F. In Dual trap q-q-time of flight mass spectrometry. *Proceedings of the 49th ASMS Conference on Mass Spectrometry and Allied Topics*, Chicago, 2001.

44. Badman ER, Hoaglund-Hyzer CS, Clemmer DE. Monitoring structural changes of proteins in an ion trap over ~10–200 ms: Unfolding transitions in cytochrome c ions. *Anal. Chem.* 2001; **73**: 6000.

45. Doroshenko VM, Cotter RJ. A quadrupole ion trap/time-of-flight mass spectrometer with a parabolic reflectron. *J. Mass Spectrom.* 1998; **33**: 305.

46. de Hoffmann E, Stroobant V. *Mass Spectrometry: Principles and Applications*, 2nd ed. John Wiley & Sons: Chichester, 2002.

47. Okumura D, Toyoda M, Ishihara M, Katakuse I. Application of a multi-turn time-of-flight mass spectrometer, multum ii, to organic compounds ionized by matrix-assisted laser desorption/ionization. *J. Mass Spectrom.* 2004; **39**: 86.

48. Sakurai T, Baril M. Ion optics of a high-resolution multipassage mass spectrometer with electrostatic ion mirrors. *Nucl. Instrum. Methods Phys. Res., Sect. A* 1995; **363**: 473.

49. Okumura D, Toyoda M, Ishihara M, Katakuse I. A compact sector-type multi-turn time-of-flight mass spectrometer 'multum ii'. *Nucl. Instrum. Methods Phys. Res., Sect. A* 2004; **519**: 331.

50. Dahl DA. *Simion 3d, Version 7.0*. Idaho national engineering laboratory: Idaho, 2001.

51. Moini M. Ultramark 1621 as a calibration/reference compound for mass spectrometry. II. Positive-and negative-ion electrospray ionization. *Rapid Commun. Mass Spectrom.* 1994; **8**: 711.

52. Senko M. Isopro 3.0. http://members.aol.com/msmssoft/2003.

53. Strupat K, Carte N, Rogniaux H, Leize E, Dorsselaer AV. Esi-iontrap-ms of biological non-covalently bound complexes: Feasibility study using an orthogonal source & comparison to esi-quadrupole-ms using a linear source. In *Proceedings of the 47th ASMS Conference on Mass Spectrometry and Allied Topics*, Dallas, 1999.

54. Rogniaux H, Sanglier S, Strupat K, Azza S, Roitel O, Ball V, Tritsch D, Branlant G, Dorsselaer AV. Mass spectrometry as a novel approach to probe cooperativity in multimeric enzymatic systems. *Anal. Biochem.* 2001; **291**: 48.

55. Hu Q, Makarov A, Noll RJ, Cooks RG. Application of the orbitrap mass analyzer to biologically relevant compounds. In *Proceedings of the 52nd ASMS Conference on Mass Spectrometry and Allied Topics*, Nashville, 2004.

56. Syka JEP, Marto JA, Bai DL, Horning S, Senko MW, Schwartz JC, Ueberheide B, Garcia B, Busby S, Muratore T, Shabanowitz J, Hunt DF. Novel linear quadrupole ion trap/ft mass spectrometer: performance characterization and use in the comparative analysis of histone h3 post-translational modifications. *J. Proteome Res.* 2004; **3**: 621.

57. Cooks RG, Zhang D, Koch KJ, Gozzo FC, Eberlin MN. Chiroselective self-directed octamerization of serine: implications for homochirogenesis. *Anal. Chem.* 2001; **73**: 3646.

58. Koch KJ, Gozzo FC, Zhang D, Eberlin MN, Cooks RG. Serine octamer metaclusters: formation, structure elucidation and implications for homochiral polymerization. *Chem. Commun.* 2001; **18**: 1854.

59. Takats Z, Nanita SC, Cooks RG, Schlosser G, Vekey K. Amino acid clusters formed by sonic spray ionization. *Anal. Chem.* 2003; **75**: 1514.

60. Takats Z, Nanita SC, Cooks RG. Serine octamer reactions: indicators of prebiotic relevance. *Angew. Chem., Int. Ed. Engl.* 2003; **42**: 3521.

61. Julian RR, Hodyss R, Kinnear B, Jarrold M, Beauchamp JL. Nanocrystalline aggregation of serine detected by electrospray ionization mass spectrometry: origin of the stable homochiral gas phase serine octamer. *J. Phys. Chem. B* 2002; **106**: 1219.

62. Schalley CA, Weis P. Unusually stable magic number clusters of serine with a surprising preference for homochirality. *Int. J. Mass Spectrom.* 2002; **221**: 9.

63. Counterman AE, Clemmer DE. Magic number clusters of serine in the gas phase. *J. Phys. Chem. B* 2001; **105**: 8092.

64. Wood TD, Chorush RA, Wampler FM, Little DP, Oconnor PB, McLafferty FW. Gas-phase folding and unfolding of cytochrome-c cations. *Proc. Natl. Acad. Sci. U.S.A.* 1995; **92**: 2451.

65. Suckau D, Shi Y, Beu SC, Senko MW, Quinn JP, Wampler FM, McLafferty FW. Coexisting stable conformations of gaseous protein ions. *Proc. Natl. Acad. Sci. U.S.A.* 1993; **90**: 790.

66. Campbell S, Rodgers MT, Marzluff EM, Beauchamp JL. Structural and energetic constraints on gas-phase hydrogen-deuterium exchange-reactions of protonated peptides with d2o, cd3od, cd3co2d, and nd3. *J. Am. Chem. Soc.* 1994; **116**: 9765.

67. Campbell S, Rodgers MT, Marzluff EM, Beauchamp JL. Deuterium exchange reactions as a probe of biomolecule structure. Fundamental studies of cas phase h/d exchange reactions of protonated glycine oligomers with d2o, cd3od, cd3co2d, and nd3. *J. Am. Chem. Soc.* 1995; **117**: 12 840.

68. Dookeran NN, Harrison AG. Gas-phase h-d exchange-reactions of protonated amino-acids and peptides with nd3. *J. Mass Spectrom.* 1995; **30**: 666.

69. Dookeran NN, Harrison AG. Reactive collisions in quadrupole cells. 3. H/d exchange-reactions of protonated aromatic-amines with nd(3). *J. Am. Soc. Mass Spectrom.* 1995; **6**: 19.

70. Ustyuzhanin P, Ustyuzhanin J, Lifshitz C. An electrospray ionization—flow tube study of h/d exchange in protonated serine. *Int. J. Mass Spectrom.* 2003; **223**: 491.

71. Freitas MA, Hendrickson CL, Emmett MR, Marshall AG. High-field fourier transform ion cyclotron resonance mass spectrometry for simultaneous trapping and gas-phase hydrogen/deuterium exchange of peptide ions. *J. Am. Soc. Mass Spectrom.* 1998; **9**: 1012.

72. Freitas MA, Marshall AG. Rate and extent of gas-phase hydrogen/deuterium exchange of bradykinins: evidence for peptide zwitterions in the gas phase. *Int. J. Mass Spectrom.* 1999; **183**: 221.

73. Hardman M, Denisov E, Makarov A. Ion fragmentation and storage in an asymmetric trapping quadrupole coupled to the orbitrap mass analyser. In *Proceedings of the 50th ASMS Conference on Mass Spectrometry and Allied Topics*, Orlando, 2002.

74. Mazurek U, Reuben BG, McFarland MA, Marshall AG, Lifshitz C. Elucidating structures of protonated amino acid clusters from H/D exchange experiments: the protonated serine octamer. In *Proceedings of the 52nd ASMS Conference on Mass Spectrometry and Allied Topics*, Nashville, 2004.

75. Li H, Cooks RJ, unpublished results, 2003.

76. Salt DE, Prince RC, Baker AJM, Raskin I, Pickering IJ. Zinc ligands in the metal hyperaccumulator thlaspi caerulescens as determined using x-ray absorption spectroscopy. *Environ. Sci. Technol.* 1999; **33**: 713.

77. Grimm CC, Grimm DA, Bergman CJ (eds). *The Analysis of Oligosaccharides by Mass Spectrometry*. American Chemical Society: Washington, 2003.

78. Zala J. Mass spectrometry of oligosaccharides. *Mass. Spectrom. Rev.* 2004; **23**: 161.

79. Cass RT, Villa JS, Karr DE, Donald E, Schmidt J. Rapid bioanalysis of vancomycin in serum and urine in hplc-tandem mass spectrometry using on-line sample extraction and parallel analytical columns. *Rapid Commun. Mass Spectrom.* 2001; **15**: 406.